https://doi.org/10.3311/PPci.39738

Periodica Polytechnica Civil Engineering

Analytical Investigation of Buckling Behavior in Bi-curved GPLs-reinforced Sandwich Composite Shells with Cellular Core

Zhifang Zhang[1], Kang Li[1*]

[1] School of Mechanical and Power Engineering, Cangzhou Jiaotong College, 061199 Cangzhou, China
[*] Corresponding author, e-mail: lkzzf_615113@163.com

Received: 28 December 2024, Accepted: 31 December 2025, Published online: 19 May 2026

Abstract

This study investigates axial buckling of sandwich composite shells with anti-tetrachiral lattice cores and graphene-reinforced surfaces, analytically deriving mechanical properties for GPL distributions: uniform (UD), V-pattern (FG-V), and X-pattern (FG-X). The fundamental formulas are formed utilizing Reddy higher-order shear deformation theory (HSDT) and minimize the total potential energy principle. The Navier solution tactic is employed to extract the characteristic equation of the system, which is subsequently resolved to calculate the critical buckling load for different geometric and mechanical parameter configurations. The results reveal that volume fraction and distribution of GPLs significantly influence the buckling load, with optimal performance being contingent upon the geometric constraints of the lattice core. By optimizing the lattice core specifications, the highest buckling load can be achieved with minimal GPL volume fraction, enhancing the economic feasibility of nanoparticle usage in such structures. Notably, the FG-V distribution with a 0.05 wt.% GPL demonstrates the most efficient configuration for maximizing the buckling load. The results emphasize the importance of optimizing the geometry of the lattice core to achieve the maximum buckling load. Specifically, for a lattice configuration with R_x/R_y = 1.5, the optimal inclination angle of 10° leads to a 0.8% increase in buckling load compared to other angles. Similarly, for R_x/R_y = 1, the highest buckling load is obtained at an inclination angle of 60°, which is approximately 30% greater than the minimum buckling load observed. These findings highlight the critical role of geometric optimization in maximizing the structural stability and performance of bi-curved sandwich composite shells.

Keywords

buckling, sandwich shell, functionally graded materials, graphene platelets, cellular structure

1 Introduction

Bi-curved sandwich panels are one of the major structural components in several applications, such as aerospace, marine, transportation, mechanical, and civil engineering, owing to their superior tensile-to-weight ratio [1–4]. Sandwich panels are usually made of two stiff outer faces – often metal or composite – combined with a lightweight core that enhances structural efficiency. The core is usually composed of low-density materials, such as porous plastics like foam or honeycomb structures, thin-walled profiles bonded to the outer layers, and latticed sheets [5]. Such a structural combination offers high stiffness and load-carrying capacity with relatively low structural weight. Those characteristics make the sandwich panels the best option for applications requiring mechanical strength and lightness. This feature is also valuable in designs where the reduction in material usage and overall weight is an objective without compromising on structural integrity [6–8].

Sandwich panels with lattice cores have been widely used in civil engineering applications due to their lightweight and high strength [9–11]. For instance, the Sandwich Plate System (SPS), consisting of two metallic plates with an elastomeric core, has been employed in projects such as the Dawson Bridge rehabilitation in Edmonton, Canada, and the construction of the Philippine Arena near Manila [4]. These structures contribute to overall weight reduction and enhanced mechanical performance, enabling more optimized structural designs.

The use of sandwich bi-curvature panels in engineering applications has been attracting growing interest from researchers in different scientific fields towards the research and evaluation of this structural class in numerous

Cite this article as: Zhang, Z., Li, K. "Analytical Investigation of Buckling Behavior in Bi-curved GPLs-reinforced Sandwich Composite Shells with Cellular Core", Periodica Polytechnica Civil Engineering, 2026. https://doi.org/10.3311/PPci.39738

aspects [12]. One of the most significant areas has been incorporating nanoparticle-reinforced materials, which can be expected to bring about significant enhancement in the material traits of the sandwich structures [13, 14]. The employment of nanoparticles, such as carbon nanotubes [15–18], nano alumina [19–21], TiO_2 nanoparticles [22, 23], and graphene platelets (GPLs) [24–26], has shown encouraging results in the strengthening of these materials, enhancing their load-bearing capacities under various conditions. Rahmani et al. [27] reviewed the vibrations of FGM core sandwich structures utilizing HSDT. Rahmani et al. [28] explored vibrations of the composite outside layers with a flexible core cylindrical sandwich shell by considering HSDT. Dastjerdi et al. [29] examined composite plates for bending through an extended Kantrovich technique utilizing HSDT. Kheirikhah et al. [30] considered the sandwich sheets to have composite outer layers and a soft core buckle. They studied how the shape and size of the structure affect its buckling behavior. Viola et al. [31] established a comprehensive scheme for the dynamics of high-thickness and bi-curved multilayered plates.

Recent studies have further advanced the understanding of cellular and composite structures. For instance, Malek and Gibson [32] provides a detailed investigation into the mechanical response of cellular materials under varying loading conditions, which is relevant to the present study. Moreover, Tornabene et al. [33] explores the structural behavior of lightweight cellular cores, contributing to the discussion on the homogenization approach. Additionally, Salehipour et al. [34] and Tornabene et al. [35] present recent advancements in composite reinforcement strategies and material optimization, which support the motivation for integrating nanoplates into composites. These references have been incorporated to provide a more comprehensive background for the study.

Chen et al. [36] examined the post-buckling reaction of bi-curved sandwich panels with transverse stiffeners. They determined the equivalent mechanical properties of the stiffened shell using static equilibrium. Lotfan et al. [37] considered the vibrations of bi-curved shells under axial motion, employing HSDT. Tornabene et al. [33] investigated the dynamics of bi-curved shells with honeycomb cores, using the finite element method under various loading conditions. Sayyad and Ghugal [38] considered the dynamics of bi-curved FGM shells using the Navier solution technique, providing insights into the impact of the material gradation on the natural frequencies of the structures. Esmaeili and Kiani [39] examined the vibrations of bi-curved shells reinforced with graphene nanosheets, which have become popular due to their excellent mechanical properties. Han et al. [40] considered the vibrations of graphene-reinforced bi-curved shells employing HSDT. They utilized the Halpin-Tsai model to define the mechanical properties of the structure and derived the equations by Hamilton's principle. These studies collectively enhance our consideration of how material composition and structural reinforcement affect the dynamics and vibrations of the bi-curved shells, particularly in advanced engineering applications.

Although intensive investigation has been performed in the domain of bi-curved panels with cellular core configurations, there is still a noticeable gap in the research on how GPL reinforcement affects the buckling behavior of bi-curvature composite panels with cellular cores. In this investigation, the buckling reaction of a bi-curvature sandwich composite panel with a cellular core and the GPLs-reinforced faces is considered analytically for the first time. The rule of mixtures is employed in determining the efficient mechanical traits of the nanocomposite faces. The formulas governing the buckling behavior of the structure are derived based on HSDT. In solving the derived equations effectively, the Navier solution method is adopted. The impact of different metrics will be systematically explored, including the geometry of the cellular core and GPL distribution, on the buckling response of the panels after verifying the analytical results. This exploration contributes to a deeper understanding of the structural productivity of composite materials in advanced engineering applications, paving the way for the optimization of designs that leverage GPL reinforcement to enhance the strength and stability of bi-curved sandwich structures.

2 Mathematical formulation

In this work, a bi-curved sandwich composite shell characterized by a lattice core and GPLs-reinforced surface layers is examined, as illustrated in Fig. 1 [41]. The dimensions are defined by the longitudinal and transverse edges, which measure a and b, correspondingly.

The curvature radii for the longitudinal and transverse directions are depicted as R_L and R_T, correspondingly, while the thickness of the core is displayed by t_c and the thickness of the outer layers by t. The coordinate system's origin is positioned at the mid-plane of the shell, with the z-axis oriented toward the curvature of the panel. The core structure is designed using a lattice configuration, depicted in Fig. 1 (b). In this design, the lengths of the diagonal sections, diagonal legs, and vertical legs are

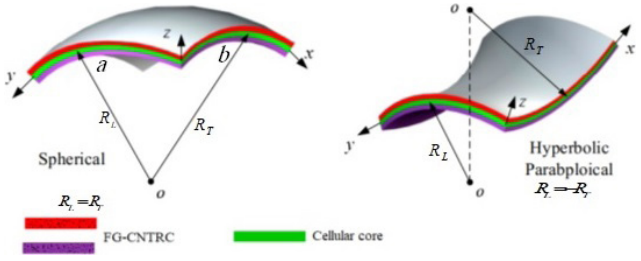

(a)

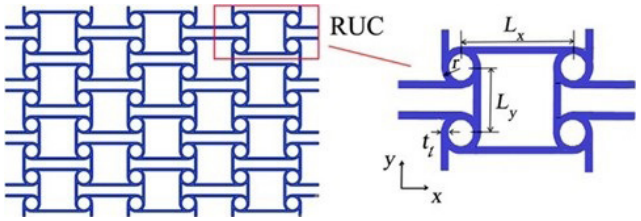

(b)

Fig. 1 Schematic configuration of the GPL-reinforced bi-curved sandwich composite shell with anti-tetrachiral cellular core: (a) Bi-curved sandwich composite shell with cellular core and GPLs-reinforced faces; (b) Anti-tetrachiral core, illustrating the unit cell and its geometrical parameters [41]

depicted as L_y and $L_x = \beta L_y$, correspondingly, while the thickness of the cross-section of the foundational elements is considered as $t_f = \alpha L_x$. Consequently, the geometric configuration of the anti-tetrachiral auxetic core cells is governed by four primary parameters: L, α, β, and r, as illustrated in Fig. 1 (b). This intricate relationship among the parameters is essential in identifying the mechanical performance and buckling characteristics of the bi-curved sandwich composite shell under various loading conditions.

2.1 Equivalent mechanical characteristics of the cellular core

This section delineates the equivalent mechanical characteristics of the lattice core, which are pivotal in identifying the overall enactment of the bi-curved sandwich composite shell. To determine the equivalent mechanical properties of the cellular core, a numerical homogenization approach was employed. In this method, a representative unit of the cellular structure was selected, and appropriate boundary conditions were applied to extract its mechanical response under various loading conditions. Subsequently, the effective elastic moduli were determined using the average stress-strain relations. Furthermore, the homogenized properties were validated by comparing them with experimental results and finite element analysis to ensure the accuracy of the proposed model.

The mechanical traits of the cellular core – namely density, Young's modulus, shear modulus, and Poisson's ratio – are derived based on the geometric parameters of the structure [42] and expressed as follows:

1. Effective density (ρ_c): the density of a cellular structure with a lattice core relies on the traits of the constituent materials and the geometric configuration of the cells. It is depicted below:

$$\rho_c = 2\frac{t_l}{l} + \left(1 + \frac{\pi}{rl}\right). \tag{1}$$

2. Effective Young modulus (E_c): the effective Young's modulus of the anti-tetrachiral core is displayed below:

$$E_c = \frac{E\lambda^3}{6(1-0.5\lambda)^2}\left(\frac{1}{\gamma - 2\sqrt{2\lambda - \lambda^2}}\right), \tag{2}$$

$$\gamma = \frac{l}{r}, \tag{3}$$

$$\lambda = \frac{t_l}{r}. \tag{4}$$

3. Effective shear modulus (G_c): the shear modulus of the anti-tetrachiral cellular core was obtained as:

$$G_c = \frac{E_c}{2(1+\nu_c)}, \tag{5}$$

where ν_c stands for Poisson's ratio of the material.

4. Effective Poisson ratio (ν_c): ν_c for the lattice core expressed as follows in Eq. (6):

$$\nu_c = -1. \tag{6}$$

2.2 Effective mechanical porosities of GPLs-reinforced surface layers

Surfaces of the bi-curved sandwich shell are reinforced with GPLs using two distinct distribution strategies: uniform distribution (UD) and functionally graded distribution (FGD).

2.2.1 Uniform distribution (UD)

In this case, GPLs are dispersed uniformly across the thickness of the top surfaces. The volume fraction of GPLs (V_{GPLs}) is represented as:

$$V_{\text{GPLs-UD}} = V_0. \tag{7}$$

In a functionally graded distribution strategy, the distribution of GPLs varies across the thickness of the composite shell, which can be categorized into two configurations:

- FG-V: in this alignment, the volume fraction of GPLs increases or decreases vertically through the thickness:

$$V_{\text{GPLs-FG-V}} = V_{GPLs}^{*}\left(1+\frac{2}{h_s}\left(z\pm\frac{h_c+h_s}{2}\right)\right). \tag{8}$$

- FG-X: here, the volume fraction of GPLs varies horizontally, allowing for a gradient effect that responds to varying stress distributions across the surface of the shell:

$$V_{\text{GPLs-FG-X}} = \frac{4}{h_s}\left|z\pm\frac{h_c+h_s}{2}\right|V_{\text{GPLs}}^{*}, \tag{9}$$

in which:

$$V_{\text{GPLs}}^{*} = \frac{w_{\text{GPLs}}}{w_{\text{GPLs}}+\left(\frac{\rho^{\text{GPLs}}}{\rho^{m}}\right)\left(1-w_{\text{GPLs}}\right)}. \tag{10}$$

The efficient mechanical traits of the GPLs-amplified surface layers can be derived using the rule of mixtures, accounting for the volume fractions and individual moduli of the GPLs and the matrix material [43]:

$$E_{11} = \eta_1 V_{\text{GPLs}} E_{11}^{\text{GPLs}} + V_m E^m, \tag{11}$$

$$E_{22} = \frac{\eta_2}{\frac{V_{\text{GPLs}}}{E_{22}^{\text{GPLs}}}+\frac{V^m}{E^m}}, \tag{12}$$

$$G_{12} = \frac{\eta_3}{\frac{V_{\text{GPLs}}}{G_{12}^{\text{GPLs}}}+\frac{V^m}{G^m}}, \tag{13}$$

$$G_{21} = G_{23} = 1.2G_{12}, \tag{14}$$

where E, G and η_i (i = 1,2,3) are the Young modules, and GPLs constants, correspondingly. The index m consistently denotes the matrix properties of the surface layers.

The density and v_c for the GPLs-reinforced surface layers are considered based on the characteristics of the matrix and the GPLs:

$$\rho_s = V_{\text{GPLs}}\rho^{\text{GPLs}} + V_m\rho^m, \tag{15}$$

$$\nu = V_{\text{GPLs}}\nu^{\text{GPLs}} + V_m\nu^m. \tag{16}$$

2.3 The HSDT

In this study, the analysis is performed under the plane stress assumption, which is appropriate for thin structures where the out-of-plane stresses are negligible.

In this section, the primary formulas for the buckling of bi-curved shells with lattice cores and GPLs-reinforced surfaces are derived. For this purpose, the HSDT presented by Reddy [44] is used. Based on this theory, the midplane displacement fields are obtained as follows:

- Transverse displacement ($w(x,y,z)$):

$$w(x,y,z) = w(x,y). \tag{17}$$

- Longitudinal displacement ($u(x,y,z)$):

$$u(x,y,z) = \left(1+\frac{z}{R_x}\right)u + \phi_1 z - \frac{4}{3h^2}\left(\phi_1+\frac{\partial w}{\partial x}\right)z^3. \tag{18}$$

- Transverse displacement ($v(x,y,z)$):

$$v(x,y,z) = \left(1+\frac{z}{R_y}\right)v + z\phi_2 - \frac{4}{3h^2}z^3\left(\phi_2+\frac{\partial w}{\partial y}\right). \tag{19}$$

where ϕ_1 and ϕ_2 stand rotation of normal vectors around the x and y axes. Also, transverse shear strains for the bi-curved shell are obtained in Eqs. (20) and (21):

$$\gamma_{xz} = \frac{\partial u}{\partial z} + \frac{1}{1+\frac{z}{R_x}}\left(\frac{\partial u_3}{\partial x}-\frac{u}{R_x}\right), \tag{20}$$

$$\gamma_{yz} = \frac{\partial v}{\partial z} + \frac{1}{1+\frac{z}{R_y}}\left(\frac{\partial u_3}{\partial y}-\frac{v}{R_y}\right). \tag{21}$$

By inserting Eqs. (18) and (19) into Eqs. (20) and (21), the third-order shear strains of Reddy theory are obtained as follows:

$$\gamma_{xz} = \left(\frac{\partial w}{\partial x}+\phi_1\right)\left(1-\frac{z}{R_x}-z^2\frac{4}{R_x h_c}+z^3\frac{4}{3R_x h_c^2}\right), \tag{22}$$

$$\gamma_{yz} = \left(\frac{\partial w}{\partial y}+\phi_2\right)\left(1-\frac{z}{R_y}-z^2\frac{4}{R_y h_c}+z^3\frac{4}{3R_y h_c^2}\right). \tag{23}$$

Using the Eqs. (17) to (23) of the strain-displacement equations of HSDT, omitting z^3 terms, equations can be displayed in Eqs. (24) to (27):

$$\varepsilon_{xx} = \varepsilon_{xx,0} + z\left(k_1^{(0)} + zk_1^{(1)} + z^2k_1^{(2)}\right), \tag{24}$$

$$\varepsilon_{yy} = \varepsilon_{yy,0} + z\left(k_2^{(0)} + zk_2^{(1)} + z^2k_2^{(2)}\right), \tag{25}$$

$$\gamma_{xy} = \gamma_{xy,0} + z\left(k_{12}^{(0)} + zk_{12}^{(1)} + z^2k_{12}^{(2)}\right), \tag{26}$$

$$\gamma_{xz} = \gamma_{xz,0} + z\left(k_{13}^{(0)} + zk_{13}^{(1)} + z^2k_{13}^{(2)}\right), \tag{27}$$

$$\gamma_{yz} = \gamma_{yz,0} + z\left(k_{23}^{(0)} + zk_{23}^{(1)} + z^2k_{23}^{(2)}\right), \tag{28}$$

where:

$$\varepsilon_{xx,0}=\frac{\partial u}{\partial x}+\frac{w}{R_x},\varepsilon_{yy,0}=\frac{\partial v}{\partial y}+\frac{w}{R_y}, \tag{29}$$

$$\gamma_{xy,0}=\frac{\partial v}{\partial x}+\frac{\partial u}{\partial y},\gamma_{xz,0}=\phi_1+\frac{\partial w}{\partial x}, \tag{30}$$

$$\gamma_{yz,0}=\phi_2+\frac{\partial w}{\partial y}, \tag{31}$$

$$k_1^{(0)}=\frac{\partial\phi_1}{\partial x}-\frac{w}{R_x^2}, \tag{32}$$

$$k_1^{(1)}=-\frac{1}{R_x}\left(\frac{\partial\phi_1}{\partial x}-\frac{1}{R_x}\frac{\partial u}{\partial x}\right), \tag{33}$$

$$k_1^{(2)}=-\frac{4}{3h_c^2}\left(\frac{\partial\phi_1}{\partial x}+\frac{\partial^2 w}{\partial x^2}\right), \tag{34}$$

$$k_2^{(0)}=\frac{\partial\phi_2}{\partial y}-\frac{w}{R_y^2},k_2^{(1)}=-\frac{1}{R_y}\left(\frac{\partial\phi_2}{\partial y}-\frac{1}{R_y}\frac{\partial v}{\partial y}\right), \tag{35}$$

$$k_2^{(2)}=-\frac{4}{3h_c^2}\left(\frac{\partial\phi_2}{\partial y}+\frac{\partial^2 w}{\partial y^2}\right), \tag{36}$$

$$k_{12}^{(0)}=\frac{\partial\phi_1}{\partial y}+\frac{\partial\phi_2}{\partial x}+\frac{\partial u}{\partial y}\left(\frac{1}{R_x}-\frac{1}{R_y}\right)+\frac{\partial v}{\partial x}\left(-\frac{1}{R_x}+\frac{1}{R_y}\right), \tag{37}$$

$$k_{12}^{(1)}=-\frac{1}{R_y}\frac{\partial\phi_1}{\partial y}-\frac{1}{R_x}\frac{\partial\phi_2}{\partial x}-\frac{1}{R_xR_y}\frac{\partial u}{\partial y}-\frac{1}{R_xR_y}\frac{\partial v}{\partial x}, \tag{38}$$

$$k_{12}^{(2)}=-\frac{4}{3h^2}\left(\frac{\partial\phi_1}{\partial y}+\frac{\partial\phi_2}{\partial x}+2\frac{\partial^2 w}{\partial x\partial y}\right), \tag{39}$$

$$k_{13}^{(0)}=-\frac{1}{R_x}\gamma_{xz,0},k_{13}^{(1)}=-\frac{4}{h^2}\gamma_{xz,0},k_{13}^{(2)}=-\frac{1}{3R_xh^2}\gamma_{xz,0}, \tag{40}$$

$$k_{23}^{(0)}=-\frac{1}{R_y}\gamma_{yz,0},k_{23}^{(1)}=-\frac{4}{h^2}\gamma_{yz,0},k_{23}^{(2)}=-\frac{1}{3R_yh^2}\gamma_{yz,0}. \tag{41}$$

According to Eq. (13), the constitutive relations for the upper, lower, and core surfaces of bi-curved shells can be obtained as follows:

$$\begin{aligned}\left\{\sigma^{(k)}\right\}&=\left[Q^{(k)}\right]\begin{Bmatrix}\varepsilon_{xx,0}\\ \varepsilon_{yy,0}\\ \gamma_{xy,0}\\ \gamma_{xz,0}\\ \gamma_{yz,0}\end{Bmatrix}+z\left[Q^{(k)}\right]\begin{Bmatrix}k_1^{(0)}\\ k_2^{(0)}\\ k_{12}^{(0)}\\ 0\\ 0\end{Bmatrix}\\&+z^2\left[Q^{(k)}\right]\begin{Bmatrix}0\\ 0\\ 0\\ k_{13}^{(1)}\\ k_{23}^{(1)}\end{Bmatrix}+z^3\left[Q^{(k)}\right]\begin{Bmatrix}k_1^{(2)}\\ k_2^{(2)}\\ k_{12}^{(2)}\\ 0\\ 0\end{Bmatrix}.\end{aligned} \tag{42}$$

where the superscript k represents the upper, and lower surfaces and core. In Eq. (13), the terms $k_{13}^{(0)}$, $k_{13}^{(2)}$, $k_{23}^{(0)}$, $k_{23}^{(2)}$, $k_1^{(1)}$, $k_2^{(1)}$ and $k_{12}^{(1)}$ have been omitted, assuming a relatively thick shell [31]. Also, the diminished stiffness modulus matrix for the k-th layer is as follows [32]:

$$\left[Q^{(k)}\right]=\begin{bmatrix}Q_{11}^k & Q_{12}^k & 0 & 0 & 0\\ Q_{21}^k & Q_{22}^k & 0 & 0 & 0\\ 0 & 0 & Q_{44}^k & 0 & 0\\ 0 & 0 & 0 & Q_{55}^k & 0\\ 0 & 0 & 0 & 0 & Q_{66}^k\end{bmatrix}, \tag{43}$$

and:

$$Q_{11}^{(k)}=\frac{E_{11}^k}{1-\nu_{12}^k\nu_{21}^k}, \tag{44}$$

$$Q_{12}^{(k)}=\frac{\nu_{12}^kE_{11}^k}{1-\nu_{12}^k\nu_{21}^k}, \tag{45}$$

$$Q_{22}^{(k)}=\frac{E_{22}^k}{1-\nu_{12}^k\nu_{21}^k}, \tag{46}$$

$$Q_{44}^{(k)}=G_{23}^k,\ Q_{55}^{(k)}=G_{13}^k,\ Q_{66}^{(k)}=G_{12}^k. \tag{47}$$

Using the principle of minimum potential energy, the primary formulas can be derived for the buckling examination of bi-curved sandwich shells with a lattice core and tops reinforced with GPLs. According to this principle, for a system in static equilibrium, the overall potential energy of the system is minimized [45–47]. The overall potential energy Π of the panel structure can be expressed as the sum of the strain energy U and the work done by external forces W:

$$\Pi=U-W. \tag{48}$$

Strain energy can be calculated by incorporating the strain energy density over the volume of the shell [48]. For a bi-curved shell, the strain energy density is provided below:

$$\begin{aligned}U=&\frac{1}{2}\sum_{n=1}^{3}\int_0^a\int_0^b\int_{h_{n-1}}^{h_n}\begin{bmatrix}\sigma_{xx}\varepsilon_{xx}+\sigma_{xy}\gamma_{xy}\\ +\sigma_{yy}\varepsilon_{yy}+\sigma_{yz}\gamma_{yz}+\sigma_{xz}\gamma_{xz}\end{bmatrix}\\&\times\left(1+z/R_x\right)\left(1+\frac{z}{R_y}\right)dxdydz.\end{aligned} \tag{49}$$

To find the equilibrium configuration of the shell, the principle of minimum potential energy is deployed, which states that:

$$\delta\Pi=\delta U-\delta W=0. \tag{50}$$

The first variation of strain energy can be obtained below:

$$\delta U = \sum_{n=1}^{3}\int_0^a\int_0^b \begin{pmatrix} N_{xx}\delta\varepsilon_x^{(0)} + M_{xx}\delta k_1^{(0)} + P_{xx}\delta k_1^{(2)} \\ +N_{yy}\delta\varepsilon_y^{(0)} + M_{yy}\delta k_2^{(0)} + P_{yy}\delta k_2^{(2)} \\ +N_{xy}\delta\gamma_{xy}^{(0)} + M_{xy}\delta k_{12}^{(0)} + P_{xy}\delta k_{12}^{(2)} \\ +K_{xx}\delta\gamma_{xz}^{(0)} + R_{xx}k_{13}^{(2)} + K_{yy}\delta\gamma_{yz}^{(0)} + R_{yy}k_{23}^{(2)} \end{pmatrix} \times\left(1+\frac{z}{R_x}\right)\left(1+\frac{z}{R_y}\right)dxdydz. \tag{51}$$

The first variation of work done by external forces is displayed below:

$$\delta W = \int_0^b\int_0^a\left(N_x^{(0)}\frac{\partial^2 w}{\partial x^2} + N_y^{(0)}\frac{\partial^2 w}{\partial y^2} + q_w\right)\delta w dxdy. \tag{52}$$

where $N_x^{(0)}$ and $N_y^{(0)}$ signify external tensile forces are applied in the x and y axes.

By inserting Eqs. (51) and (52) in Eq. (48) and setting the coefficients δu, δv, δw, $\delta\phi_x$ and $\delta\phi_y$ to zero, there is:

$$\delta u:\ \frac{\partial N_x}{\partial x} + \frac{\partial N_{xy}}{\partial y} + N_x^{(0)} = 0, \tag{53}$$

$$\delta v:\ \frac{\partial N_{xy}}{\partial x} + \frac{\partial N_y}{\partial y} + N_y^{(0)} = 0, \tag{54}$$

$$\delta w:\ \frac{\partial K_{xz}}{\partial x} + \frac{\partial K_{yz}}{\partial y} + s_1\left(\frac{\partial^2 P_x}{\partial x^2} + 2\frac{\partial^2 P_y}{\partial x\partial y} + \frac{\partial^2 P_y}{\partial y^2}\right) - s_2\left(\frac{\partial R_{xz}}{\partial x} + \frac{\partial R_{yz}}{\partial y}\right) - \frac{N_x}{R_x} - \frac{N_y}{R_y} + N_x^{(0)}\frac{\partial^2 w}{\partial x^2} + N_y^{(0)}\frac{\partial^2 w}{\partial y^2} + q_w = 0, \tag{55}$$

$$\delta\phi_x:\ \frac{\partial \bar{M}_{xy}}{\partial y} + \frac{\partial \bar{M}_x}{\partial x} - \bar{K}_{xz} = 0, \tag{56}$$

$$\delta\phi_y:\ \frac{\partial \bar{M}_{xy}}{\partial x} + \frac{\partial \bar{M}_y}{\partial y} - \bar{K}_{yz} = 0. \tag{57}$$

where:

$$\bar{M}_i = M_i - s_1 P_i\left(i = x, y, xy\right), \tag{58}$$

$$s_1 = \frac{4}{3h^2}, \tag{59}$$

$$s_2 = 3s_1, \tag{60}$$

$$\bar{K}_{iz} = K_{iz} - s_2 R_{iz}\left(i = x, y\right). \tag{61}$$

The moment and force resultants of the shell can be obtained in Eqs. (62) to (65):

$$\left(N_x, M_x, P_x\right) = \sum_{k=1}^{K}\int_{h^{(k-1)}}^{h^{(k)}}\sigma_x\left(1, z, z^3\right)\left(1+\frac{z}{R_x}\right)dz, \tag{62}$$

$$\left(N_y, M_y, P_y\right) = \sum_{k=1}^{K}\int_{h^{(k-1)}}^{h^{(k)}}\sigma_y\left(1, z, z^3\right)\left(1+\frac{z}{R_y}\right)dz, \tag{63}$$

$$\left(N_{xy}, M_{xy}, P_{xy}\right) = \sum_{k=1}^{K}\int_{h^{(k-1)}}^{h^{(k)}}\sigma_{xy}\left(1, z, z^3\right)\left(1+\frac{z}{R_x}\right)dz, \tag{64}$$

$$\left(K_{xz}, R_{xz}\right) = \sum_{k=1}^{K}\int_{h^{(k-1)}}^{h^{(k)}}\sigma_{xz}\left(1, z^2\right)dz, \quad \left(K_{yz}, R_{yz}\right) = \sum_{k=1}^{K}\int_{h^{(k-1)}}^{h^{(k)}}\sigma_{yz}\left(1, z^2\right)dz, \tag{65}$$

where $K = 3$ is the total count of layers and $\left(h^{(k-1)}, h^{(k)}\right)$ displays the distance of k-th layer surfaces from the middle plane of the composite shell.

By employing the minimum potential energy principle, a robust foundation is established for analyzing the mechanical behavior of bi-curved sandwich shells reinforced with GPLs. This method enhances our understanding of the stability and bearing capacity of such structures and aids in optimizing their design for applications in various engineering fields.

2.4 Solution

The Navier solution technique is deployed to solve the equations. Accordingly, considering the simple supported boundary conditions, there are:

$$u\left(x,0\right) = u\left(x,b\right) = v\left(0,y\right) = v\left(a,y\right) = 0, \tag{66}$$

$$w\left(x,0\right) = w\left(x,b\right) = w\left(0,y\right) = w\left(a,y\right) = 0, \tag{67}$$

$$\phi_x\left(x,0\right) = \phi_x\left(x,b\right) = \phi_y\left(0,y\right) = \phi_y\left(a,y\right) = 0, \tag{68}$$

$$N_x\left(x,0\right) = N_x\left(x,b\right) = N_y\left(0,y\right) = N_y\left(a,y\right) = 0, \tag{69}$$

$$\bar{M}_x\left(x,0\right) = \bar{M}_x\left(x,b\right) = \bar{M}_y\left(0,y\right) = \bar{M}_y\left(a,y\right) = 0. \tag{70}$$

Thus, in light of the aforementioned boundary conditions, the displacement fields are represented below:

$$u\left(x,y\right) = \sum_{n=1}^{\infty}\sum_{m=1}^{\infty}U_{mn}\cos\left(\frac{n\pi x}{a}\right)\sin\left(\frac{m\pi x}{b}\right), \tag{71}$$

$$v\left(x,y\right) = \sum_{n=1}^{\infty}\sum_{m=1}^{\infty}V_{mn}\sin\left(\frac{n\pi x}{a}\right)\cos\left(\frac{m\pi x}{b}\right), \tag{72}$$

$$w\left(x,y\right) = \sum_{n=1}^{\infty}\sum_{m=1}^{\infty}W_{mn}\sin\left(\frac{n\pi x}{a}\right)\sin\left(\frac{m\pi x}{b}\right), \tag{73}$$

$$\phi_x\left(x,y\right) = \sum_{n=1}^{\infty}\sum_{m=1}^{\infty}\phi_{x,mn}\cos\left(\frac{n\pi x}{a}\right)\sin\left(\frac{m\pi x}{b}\right), \tag{74}$$

$$\phi_y(x,y)=\sum_{n=1}^{\infty}\sum_{m=1}^{\infty}\phi_{y,mn}\sin\left(\frac{n\pi x}{a}\right)\cos\left(\frac{m\pi x}{b}\right), \tag{75}$$

where U_{mn}, V_{mn}, W_{mn}, $\phi_{x,mn}$ and $\phi_{y,mn}$ are the unknown coefficients corresponding to the buckling modes m and n in the x and y directions, correspondingly.

Replacing Eqs. (71) to (75) with Eqs. (53) to (57) using the Navier solution method, there are:

$$L_{11}U_{mn}+L_{12}V_{mn}+L_{13}W_{mn}+L_{14}\phi_{x,mn}=0, \tag{76}$$

$$L_{21}U_{mn}+L_{22}V_{mn}+L_{23}W_{mn}+L_{24}\phi_{x,mn}+L_{25}\phi_{y,mn}=0, \tag{77}$$

$$L_{31}U_{mn}+L_{32}V_{mn}+L_{33}W_{mn}+L_{34}\phi_{x,mn}+L_{35}\phi_{y,mn}=0, \tag{78}$$

$$L_{41}U_{mn}+L_{42}V_{mn}+L_{43}W_{mn}+L_{44}\phi_{x,mn}+L_{45}\phi_{y,mn}=0, \tag{79}$$

$$L_{51}U_{mn}+L_{52}V_{mn}+L_{53}W_{mn}+L_{54}\phi_{x,mn}+L_{55}\phi_{y,mn}=0. \tag{80}$$

To identify the buckling loads of the bi-curved sandwich shell structure, the system of homogeneous algebraic equations represented by Eq. (81) is first considered. For the system to have a nontrivial (nonzero) resolution, the determinant of the coefficient matrix must be zero [49–51]. This condition leads us to formulate the characteristic equation, which is crucial for evaluating the buckling reaction of the configuration [52–54].

The characteristic equation is derived based on the governing differential equations of the system, considering the equilibrium conditions and boundary constraints. Assuming small deformations and linear elastic behavior, the equation governing the structural response can be expressed as:

$$\det\left(\begin{bmatrix} L_{11} & L_{12} & L_{13} & L_{14} & L_{15}\\ L_{21} & L_{22} & L_{23} & L_{24} & L_{25}\\ L_{31} & L_{32} & L_{33} & L_{34} & L_{35}\\ L_{41} & L_{42} & L_{43} & L_{44} & L_{45}\\ L_{51} & L_{52} & L_{53} & L_{54} & L_{55}\end{bmatrix}\right)=0. \tag{81}$$

The elements of this matrix typically contain contributions from bending stiffness, shear stiffness, as well as the influence of the geometrical constraints imposed by the bi-curvature form and its raw materials. One can then find the critical buckling loads P_{cr} by seeking the roots of the characteristic polynomial. The roots of this equation determine the fundamental behavior of the system. The derivation follows standard variational principles, incorporating compatibility conditions and constitutive relations for bi-curved GFRP-Reinforced sandwich composite shells. The lowest positive eigenvalue of this polynomial gives the critical load corresponding to the onset of buckling of the shell. This parameter is of greatest importance in considering the stability and structural integrity of sandwich composite panels under various loading.

3 Results

In this part, the impact of several metrics on the buckling load of the bi-curvature sandwich composite panel is presented for simply supported boundary conditions. To compare and discuss the outcomes, the dimensionless buckling load is used, which is depicted in Eq. (82):

$$P_{cr}=P\frac{E_c h_c^2}{R_x^2\sqrt{3\left(1-\nu_c\right)}}. \tag{82}$$

The matrix material in faces is typically a polymer amplified with GPLs. The mechanical traits of the matrix material can be summarized as:

$$E_m=2.6\ \text{GPa},\ \nu_m=0.32,\ \rho_m=1185\frac{\text{kg}}{\text{m}^3}. \tag{83}$$

GPLs are known for their exceptional mechanical properties. The relevant characteristics for the analysis can be approximated as follows:

$$\begin{aligned} &E_{11}^{\text{GPLs}}=5.64\ \text{TPa},\ E_{22}^{\text{GPLs}}=7.05\ \text{TPa},\\ &G_{12}^{\text{GPLs}}=1.945\ \text{TPa},\ \nu^{\text{GPLs}}=0.176,\\ &\eta_1=0.15,\ \eta_2=0.941,\ \eta_3=1.04. \end{aligned} \tag{84}$$

The lattice core is a crucial component of the sandwich structure, contributing to its overall stability and load-bearing capacity. The mechanical characteristics of a lattice core can be defined as follows:

$$E_c=2.32\ \text{GPa},\ \nu_c=0.34,\ \rho_c=1450\frac{\text{kg}}{\text{m}^3}. \tag{85}$$

These properties will be influenced by the geometry of the lattice structure and the material used, impacting the overall mechanical performance of the bi-curved sandwich composite shell.

In addition, in extracting all the results, the numerical default values of the geometric parameters are: $h_s=1$ mm, $h_c=4$ mm, $R_L/a=R_T/a=2$, $a=b=100\,h_c$, and $w_{\text{GPLs}}=1\%$. Four types of compound bi-curvature panels, including hyperbolic parabolic ($R_L/R_T=-1$), elliptical parabolic ($R_L/R_T=1.5$), spherical ($R_L/R_T=1$), and cylindrical ($R_L/R_T=\infty$) shells, are investigated. Also, in the default mode, the distribution type of nanoparticles is FG-X with a volume fraction of 0.1.

To validate the buckling load obtained from the current analysis, the studies conducted by Sharan [55] and Librescu et al. [56] have been referenced. For a fair comparison, the

same geometric and mechanical specifications utilized in these studies were employed in our analysis. Table 1 [55, 56] summarizes the buckling load results obtained from our analysis alongside those reported in the referenced studies. The alignment of our findings with those from Sharan [55] and Librescu et al. [56] demonstrates the precision and reliability of the analytical approach adopted in this research. As illustrated in Table 1, there is a strong correlation between the buckling load values derived in our work and those stated in Sharan [55] and Librescu et al. [56]. The consistency shows that there is robustness to our analytical model and that these methods are appropriate in investigating buckling performance for a sandwich composite shell with a bi-curved lattice core and GPLs-amplified top faces.

3.1 The effect of the geometry of the lattice core

The geometrical arrangement of the lattice core cells significantly affects the buckling behavior of bi-curved sandwich composite shells. These geometrical characteristics can be generally defined with three principal parameters: the inclination angle, cell size, and core structure thickness. All these parameters play a dissimilar role in the variation in buckling load.

In this study, the optimum configuration refers to the design that achieves the highest buckling load. The optimization process was conducted by evaluating multiple configurations with varying geometric and mechanical parameters. The configuration that exhibited the maximum buckling load was considered the optimal one.

Table 2 illustrates the angle of inclination (θ) of the lattice core components concerning the corresponding buckling load of the shell at a variety of cell size parameters. The results indicate that there is an intricate relationship between angle and buckling load and further highlight the critical need for optimization of core geometry during design. The impact of angle (θ) on the buckling load generally shows high variability. At some cell sizes, the angle has a negligible influence on buckling capacity, while in others, it becomes of paramount importance. Of special interest, at an inclination angle of 10°, the buckling load elevates by about 0.8% compared to the minimum measured buckling load for other angles. The results show an optimal angle of inclination at which the buckling load is maximum for any configuration. The determination of such an angle is important so that, under compressive loading, the structure should not fail in terms of stability. For example, for $R_x/R_y = 1.5$ the angle does not have much influence on the buckling capacity, and the highest amount of buckling load occurs at an angle of 10°, which is about 0.8% more than the lowest amount of buckling load.

Table 1 Comparison of buckling loads

Curvature	Present work	HSDT [55]	FSDT [56]	HSDT [56]
$R_x/a = 5$, $R_y/a = 5$	12.456	12.236	11.822	12.007
$R_x/a = 10$, $R_y/a = 5$	11.945	11.861	11.479	11.697
$R_x/a = 10$, $R_y/a = 20$	11.748	11.797	11.409	11.610
Plate	11.724	11.753	11.353	11.555

Table 2 Influence of inclination angle on buckling load for $\alpha = 0.5$, $\beta = 1$, $L = 0.02$

R_x/R_y	θ				
	10	30	60	80	85
1.5	15.646	15.521	15.523	15.573	15.592
1	5.924	5.616	7.315	6.093	6.048
0.5	1.371	1.272	1.271	1.316	1.330
0.3	0.229	0.133	0.131	0.176	0.189
−0.3	0.527	0.526	0.526	0.525	0.526
−0.5	1.669	1.666	1.666	1.666	1.667
−1	7.024	7.009	7.011	7.014	7.015
−1.5	15.946	15.914	15.919	15.927	15.929

In the analysis of the buckling performance of the bi-curvature sandwich panels, the angle of inclination (θ) of the lattice core members demonstrates a major influence on the buckling load. Specifically, when considering a cell configuration represented as $R_x/R_y = 1$, the highest buckling load is achieved at an angle of 60°, resulting in a buckling load approximately 30% greater than the minimum observed value. The varying effects of cell angles on the buckling load have been depicted in Fig. 2. The results illustrate that lower values of α do not influence the buckling capacity of the panel. However, as the value of α increases, there

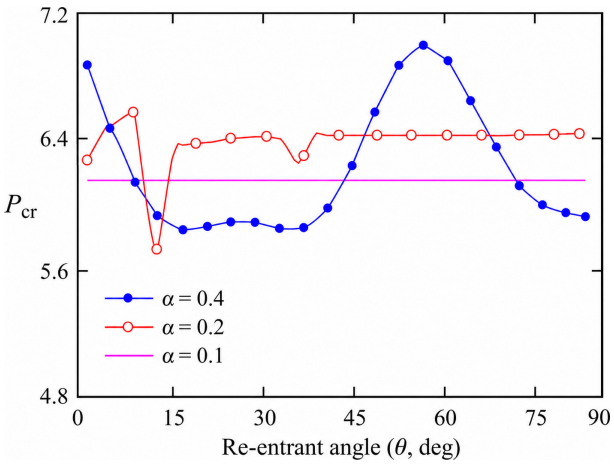

Fig. 2 Influence of inclination angle on buckling load for varying α

is a pronounced change in the buckling behavior of the system. For configurations $\alpha = 0.4$ and $\alpha = 0.2$, the maximum buckling loads correspond to specific angles, namely $\theta = 56.6°$ and $\theta = 11.6°$, correspondingly. In the best-case scenario, these angles lead to a 36% increase in the buckling load compared to other configurations.

Fig. 3 further supports these findings by showcasing that for each value of β, there exists an optimal angle θ that maximizes the buckling load. This relationship emphasizes the necessity of tuning the angle of the core members to achieve the best structural performance. The ideal values of β and θ for maximizing buckling loads are displayed in Fig. 4. Drawing on the outcomes, the highest buckling load is obtained with configurations $\theta = 25.5°$ and $\beta = 0.9$, yielding a maximum load value of 7.35.

3.2 Influence of nanocomposite shell parameters

This section presents the influences of some parameters related to the nanocomposite shell on the buckling capacity of a bi-curved sandwich composite structure. The considered parameters are curvature, aspect ratio, volume fraction, and the way nanoparticles are distributed. All these parameters are essential in determining the structural integrity and effectiveness of the composite shell.

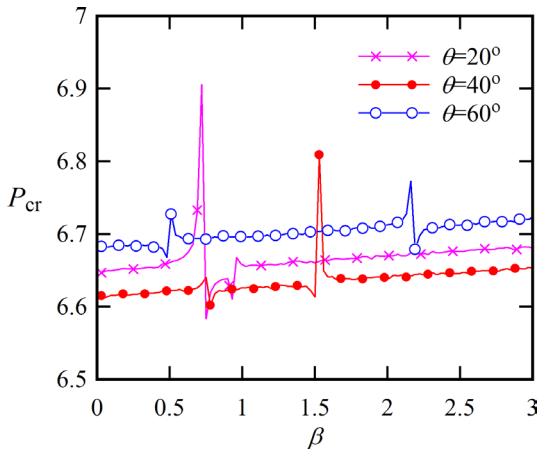

Fig. 3 Optimal cell angle for maximum buckling load across different values of θ

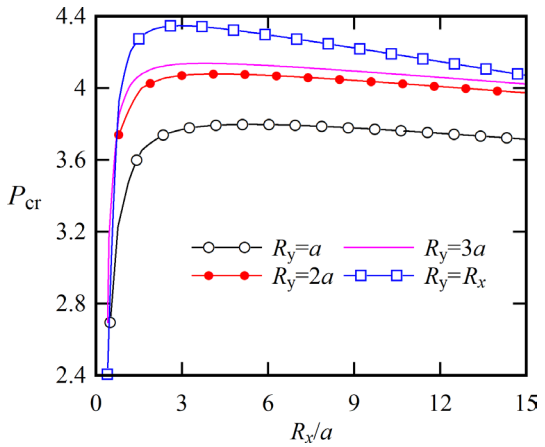

Fig. 4 The impact of curvature on the buckling capacity of the panel with two curvatures for diverse values of R_x/a

3.2.1 Effect of curvature on buckling load

The geometric curvature of a nanocomposite shell plays a vital role in determining its mechanical characteristics. On increasing the curvature, the buckling load generally shows a non-linear behavior, which may contribute to the enhancement of the structural stability of the shell. This section deals with the correlation of different curvatures and the load-bearing capability of the shell, hence serving valuable perspectives on ideal design configurations to achieve superior performance. Furthermore, the curvature radius of the shells significantly affects the buckling load in bi-curved composite structures. Fig. 5 illustrates the impact of curvature on the dimensionless buckling load P_{cr} of the double curvature shell for various values of $R_y > 0$ and $R_y < 0$. The results indicate that, in both scenarios examined, the impact of the shell's curvature on the buckling capacity is relatively minimal. As R_T increases, the buckling load shows an upward trend in both modes, with the highest buckling load achieved in the $R_L/a \geq 6$ mode. Furthermore, the case represented by $R_T = -a$, a specific value R_x/a leads to a peak in the buckling load. Beyond this optimal point, the buckling load decreases, ultimately converging to a constant value at higher parameters. This behavior aligns with the structural characteristics of thinner shells, where reduced thickness correlates with smaller critical loads. These findings underscore the importance of carefully considering curvature in the design of bi-curved composite shells to optimize their performance under buckling conditions.

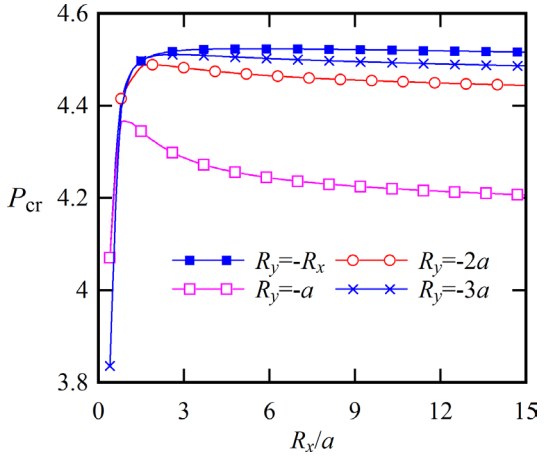

Fig. 5 The impact of curvature on the buckling capacity of the panel with two curvatures for diverse values of R_x/a

3.2.2 Effect of aspect ratio on buckling capacity

The aspect ratio, defined as the ratio of the shell's length to its height, is another crucial parameter that affects the buckling behavior. Analyzing different aspect ratios reveals how elongation or compression of the shell impacts the distribution of stress and the overall stability. This relationship is explored to identify optimal aspect ratios that maximize the buckling load. Fig. 6 illustrates the impact of the shell aspect ratio a/b on the buckling load for various values of R_L/R_T. The findings indicate that the square-shaped shell, corresponding to the a/b = 1 condition exhibits the highest buckling load. Conversely, in the case of a/b = 1.4 as the geometric dimensions of the shell transitioning towards a rectangular shape, there is a significant reduction in the buckling capacity – approximately 71% lower compared to the square-shaped shell.

Additionally, the results reveal that the parabolic hyperbolic shell configuration (i.e., $R_L/R_T = -1$) demonstrates the highest buckling capacity, while the lowest buckling load is observed in the R_L/R_T = 0.5 mode. This highlights the critical role that the aspect ratio plays in the structural integrity and performance of bi-curved composite shells under buckling conditions, emphasizing the advantages of maintaining optimal geometric dimensions.

3.2.3 Influence of volume fraction and distribution of nanoparticles

The volume fraction of GPLs within the nanocomposite shell directly influences its mechanical properties, including stiffness and strength. This analysis examines the correlation between the volume fraction of nanoparticles and the resulting buckling load, establishing guidelines for effective reinforcement through strategic material composition. The method of distributing nanoparticles – whether UD or functionally graded distribution (FG-V and FG-X) – also has significant implications for the structural performance of the shell. This section evaluates the impact of diverse spread models on mechanical behavior and buckling load, highlighting the advantages of tailored reinforcement strategies. Figs. 7 to 9 illustrate the effects of GPL distribution concerning two parameters, β and R_x/a, across various volume fractions of GPLs.

Results indicate that the increase in the radius of curvature of the shell makes the buckling load converge toward a defined value for all the scenarios analyzed. Interestingly, apart from the case of an FG-V distribution at a volume fraction of 0.02% GPLs, the buckling characteristics exhibit a considerable extent of independence from the radius of curvature. Furthermore, the buckling load rises by raising the GPL's volume fraction, as it enhances the equivalent stiffness of the structure. More specifically for FG-X distribution, the highest recorded buckling loads are 6.4 and 6.9 when the volume fraction of GPLs is elevated from 0.02 to 0.2, correspondingly, as shown in Fig. 7. Such a phenomenon marks the high

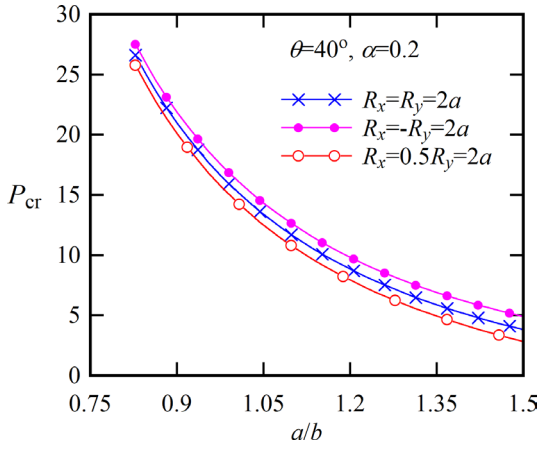

Fig. 6 The effect of the a/b on buckling load for different values of R_L/R_T

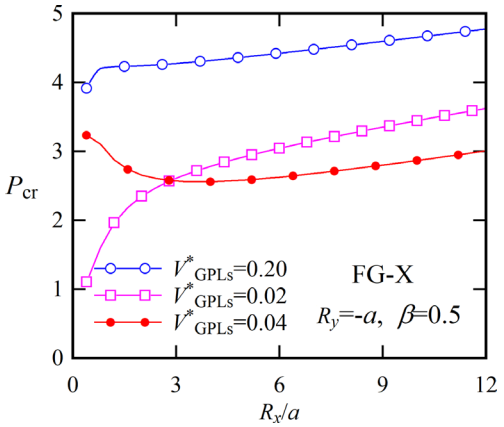

(a)

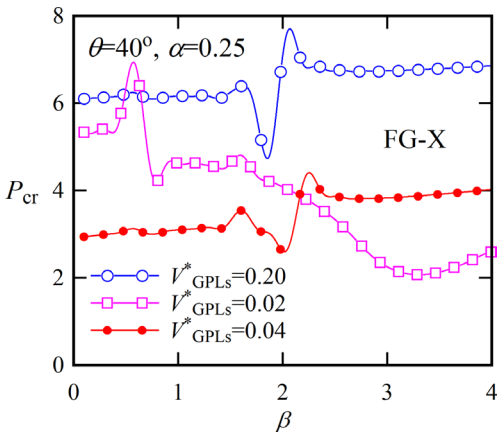

(b)

Fig. 7 Influence of FG-X distribution on buckling trait for diverse values of volume fractions of GPLs: (a) $R_y = -a$, $\beta = 0.5$; (b) $\theta = 40°$, $\alpha = 0.25$

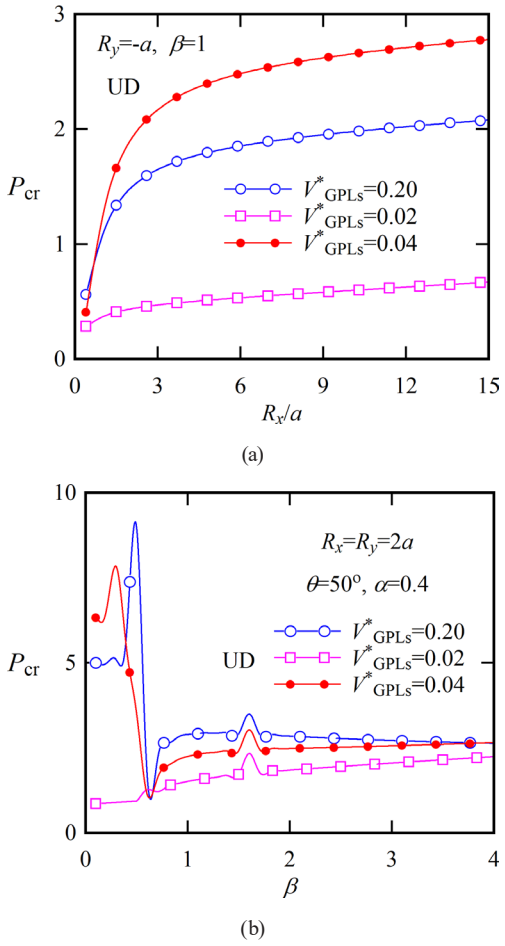

Fig. 8 Influence of UD distribution on buckling trait for diverse values of volume fractions of GPLs: (a) $R_y = -a$, $\beta = 1$; (b) $\theta = 50°$, $\alpha = 0.4$

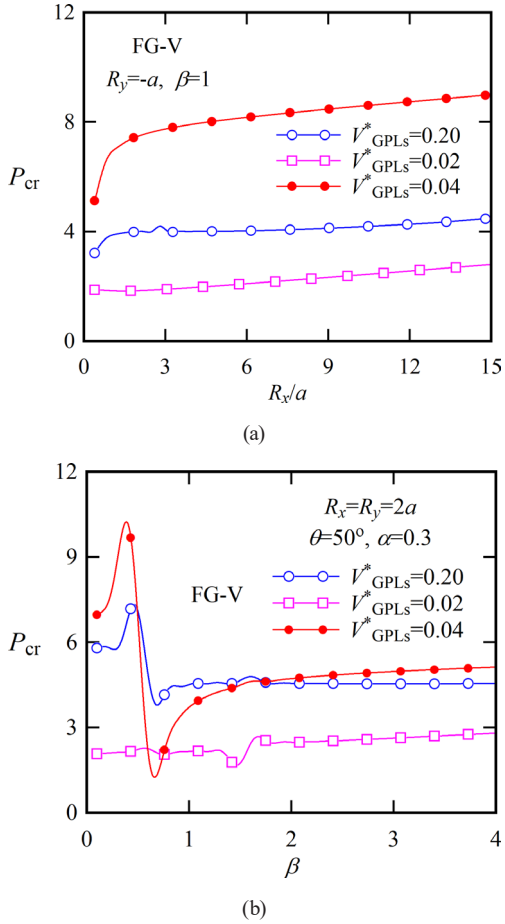

Fig. 9 Influence of FG-V distribution on buckling trait for diverse values of volume fractions of GPLs: (a) $R_y = -a$, $\beta = 1$; (b) $\theta = 50°$, $\alpha = 0.3$

importance of nanocomposite reinforcement in improving the mechanical efficacy of the bi-curved shells.

One of the key findings of this exploration is that the influence of GPL volume fraction and spread on buckling load remains relatively uncertain; the optimal performance for any such system depends strongly on the geometrical parameters defining the lattice core. By finding the optimal values for the lattice core properties, maximum buckling loads using the minimum use of GPLs can be reached. It's therefore economically beneficial to include nanoparticles when reinforcing these structures. Moreover, it is obtained from the results that the FG-V spread has the most positive impact on enhancing the mechanical properties of bi-curved shells, considerably increasing their buckling capabilities. Especially, the most obtained buckling loads related to the UD, FG-X, and FG-V spreads are 8.7, 6.9, and 10.8, accordingly, when the GPLs volume fractions are 0.2, 0.02, and 0.04, accordingly. This means that in FG-V, the optimal configuration to maximize the buckling load can be obtained with a reduced number of GPLs.

4 Conclusions

The mechanical behavior of bi-curved sandwich composite shells with lattice cores and GPLs-reinforced surfaces, under various conditions concerning buckling, is investigated. The result demonstrates the critical role that geometrical parameters, including lattice arrangement and shell curvature, play in the overall buckling load. Through comprehensive analysis, it has been demonstrated that the angle and geometry of the lattice core notably impact the buckling response, with optimal configurations leading to substantial increases in load-bearing capacity. Moreover, the reinforcement of the faces with GPLs, particularly in the functionally graded-V (FG-V) distribution, enhances the mechanical properties and provides a notable improvement in buckling loads. The maximum buckling loads for the shells reinforced with GPLs are 98.7, 6.9, and 10.8 for UD, FG-X, and FG-V distributions, accordingly, corresponding to volume fractions of 0.2, 0.02, and 0.04. These results indicate that the FG-V distribution provides the highest buckling load while requiring a lower volume

fraction of GPLs, highlighting it as the most optimal configuration for enhancing the buckling performance of the shells with minimal material use.

The results indicate that by a proper choice of lattice core parameters and setting of the GPLs, it was possible to effectively increase the buckling loads and significantly decrease the material consumption while providing a cheap solution for structure improvement. Concluding the current research provides substantial information on the progress of fresh composite materials and opens the way for their application in aerospace, automotive, and civil engineering, where high structural integrity and performance need to be maintained. The natural next step in this research field should be the investigation of dynamic behavior and longevity characteristics of these composite shells under real operating conditions to help enhance the knowledge base relating to their practical applications.

Acknowledgement

This work was supported by the Cangzhou Municipal Bureau of Science and Technology "Analytical Investigation of Buckling Behavior in Bicurved CNT-Reinforced Sandwich Composite Shells with Cellular Core" (Grant No. 23244101011).

References

[1] Fazilati, J., Khalafi, V., Jalalvand, M. "Panel flutter analysis of nano-hybrid laminated composite quadrilateral plates presuming curvilinear fibers", Mechanics Based Design of Structures and Machines, 52(10), pp. 8198–8215, 2024. https://doi.org/10.1080/15397734.2024.2316870

[2] Darakhsh, A., Rahmani, S., Amirabadi, H., Sarafraz, M., Afshari, H. "Dynamics of a three-phase polymer/fiber/CNT laminated nanocomposite conical shell with nonuniform thickness", Journal of the Brazilian Society of Mechanical Sciences and Engineering, 46(1), 40, 2024. https://doi.org/10.1007/s40430-023-04577-0

[3] Noroozi, M., Zajkani, A., Ghadiri, M. "Dynamic plastic impact behavior of CNTs/fiber/polymer multiscale laminated composite doubly curved shells", International Journal of Mechanical Sciences, 195, 106223, 2021. https://doi.org/10.1016/j.ijmecsci.2020.106223

[4] Bilir, T., Aygun, B. F., Shi, J., Gencel, O., Ozbakkaloglu, T. "Influence of Different Types of Wastes on Mechanical and Durability Properties of Interlocking Concrete Block Paving (ICBP): A Review", Sustainability, 14(7), 3733, 2022. https://doi.org/10.3390/su14073733

[5] Tornabene, F., Viscoti, M., Dimitri, R. "Higher Order Theories for Laminated Doubly-Curved Shells with Arbitrary Loads and General Boundary Conditions", In: International Conference of Steel and Composite for Engineering Structures (ICSCES 2023), Lecce, Italy, 2023, pp. 182–190. ISBN 978-3-031-57224-1 https://doi.org/10.1007/978-3-031-57224-1_18

[6] Ebrahimi-Mamaghani, A., Koochakianfard, O., Rafiei, M., Alibeigloo, A., Dizaji, A. S., Borjalilou, V. "Machine Learning, Analytical, and Numerical Techniques for Vibration Analysis of Submerged Porous Functional Gradient Piezoelectric Microbeams with Movable Supports", International Journal of Structural Stability and Dynamics, 26(09), 2650054, 2024. https://doi.org/10.1142/S0219455426500549

[7] Ebrahimi Mamaghani, A., Zohoor, H., Firoozbakhsh, K., Hosseini, R. "Dynamics of a running below-knee prosthesis compared to those of a normal subject", Journal of Solid Mechanics, 5(2), pp. 152–160, 2013. [online] Available at: https://oiccpress.com/jsm/article/view/12427 [Accessed: 20 December 2025]

[8] Ebrahimi-Mamaghani, A., Koochakianfard, O., Mostoufi, N., Khodaparast, H. H. "Dynamics of spinning pipes conveying flow with internal elliptical cross-section surrounded by an external annular fluid by considering rotary inertia effects", Applied Mathematical Modelling, 120, pp. 330–354, 2023. https://doi.org/10.1016/j.apm.2023.03.043

[9] He, L., Maalla, A., Zhou, X., Tang, H. "Buckling and post-buckling of anisogrid lattice-core sandwich plates with nanocomposite skins", Thin-Walled Structures, 199, 111828, 2024. https://doi.org/10.1016/j.tws.2024.111828

[10] Bayldon, J., Bažant, Z. P., Daniel, I. M., Yu, Q. "Size Effect on Compressive Strength of Sandwich Panels with Fracture of Woven Laminate Facesheet", Journal of Engineering Materials and Technology, 128(2), pp. 169–174, 2006. https://doi.org/10.1115/1.2172277

[11] Dolatshahi, A., Molladavoodi, H. "Specimens Size Effect on Mechanical and Fracture Properties of Rocks: a Review", Journal of Mining and Environment, 14(4), pp. 1273–1293, 2023. https://doi.org/10.22044/jme.2023.12948.2350

[12] Qi, Y.-N., Dai, H.-L., Deng, S.-T. "Thermoelastic analysis of stiffened sandwich doubly curved plate with FGM core under low velocity impact", Composite Structures, 253, 112826, 2020. https://doi.org/10.1016/j.compstruct.2020.112826

[13] Ghadiri Rad, M. H., Hosseini, S. M. "Buckling analysis of multilayer FG-CNT reinforced nanocomposite cylinders assuming CNT waviness, agglomeration, and interphase effects using the CUF-EFG method", Mechanics of Advanced Materials and Structures, 30(7), pp. 1309–1325, 2023. https://doi.org/10.1080/15376494.2022.2030443

[14] Chakraborty, S., Dey, T. "Thermomechanical buckling and wrinkling characteristics of softcore sandwich panels with CNT reinforced composite face sheets", European Journal of Mechanics - A/Solids, 98, 104894, 2023. https://doi.org/10.1016/j.euromechsol.2022.104894

[15] Pouraminian, M., Akbari Baghal, A. E., Andalibi, K., Khosravi, F., Arab Maleki, V. "Enhancing the pull-out behavior of ribbed steel bars in CNT-modified UHPFRC using recycled steel fibers from waste tires: a multiscale finite element study", Scientific Reports, 14(1), 19939, 2024.
https://doi.org/10.1038/s41598-024-68682-3

[16] Hoseinzadeh, M., Pilafkan, R., Maleki, V. A. "Size-dependent linear and nonlinear vibration of functionally graded CNT reinforced imperfect microplates submerged in fluid medium", Ocean Engineering, 268, 113257, 2023.
https://doi.org/10.1016/j.oceaneng.2022.113257

[17] Vahidi Pashaki, P., Pouya, M., Maleki, V. A. "High-speed cryogenic machining of the carbon nanotube reinforced nanocomposites: Finite element analysis and simulation", Proceedings of the Institution of Mechanical Engineers, Part C: Journal of Mechanical Engineering Science, 232(11), pp. 1927–1936, 2018.
https://doi.org/10.1177/0954406217714012

[18] Rezaee, M., Maleki, V. A. "An analytical solution for vibration analysis of carbon nanotube conveying viscose fluid embedded in visco-elastic medium", Proceedings of the Institution of Mechanical Engineers, Part C: Journal of Mechanical Engineering Science, 229(4), pp. 644–650, 2015.
https://doi.org/10.1177/0954406214538011

[19] Khameneh-asl, S., Farzaneh, A., Teymourinia, H., Mermer, O., Hosseini, M. G. "Preparation of a Ni–Mo–P–PCTFE nanocomposite coating and evaluation of its nano-tribological, mechanical and electrochemical performance", RSC Advances, 6(82), pp. 78774–78783, 2016.
https://doi.org/10.1039/C6RA12970F

[20] Farzaneh, A., Ahmad, Z., Can, M., Okur, S., Mermer, O., Havare, A. K. "The role of hydrophobicity in the development of aluminum and copper alloys for industrial applications", In: Ahmad, Z. (ed.) New Trends in Alloy Development, Characterization and Application, IntechOpen, 2015, pp. 239–266. ISBN 978-953-51-2171-8
https://doi.org/10.5772/60724

[21] Ahmad, Z., Farzaneh, A., Aleem, B. J. A. "Corrosion Behavior of Aluminium Metal Matrix Composite", In: Ahmad, Z. (ed.) Recent Trends in Processing and Degradation of Aluminium Alloys, IntechOpen, 2011, pp. 385–406. ISBN 978-953-307-734-5
https://doi.org/10.5772/23631

[22] Farzaneh, A., Esrafili, M. D., Mermer, Ö. "Development of TiO_2 nanofibers based semiconducting humidity sensor: adsorption kinetics and DFT computations", Materials Chemistry and Physics, 239, 121981, 2020.
https://doi.org/10.1016/j.matchemphys.2019.121981

[23] Farzaneh, A., Mohammadzadeh, A., Esrafili, M. D., Mermer, O. "Experimental and theoretical study of TiO_2 based nanostructured semiconducting humidity sensor", Ceramics International, 45(7), pp. 8362–8369, 2019.
https://doi.org/10.1016/j.ceramint.2019.01.144

[24] Pourreza, T., Alijani, A., Maleki, V. A., Kazemi, A. "The effect of magnetic field on buckling and nonlinear vibrations of Graphene nanosheets based on nonlocal elasticity theory", International Journal of Nano Dimension, 13(1), pp. 54–70, 2022.
https://doi.org/10.22034/ijnd.2022.683988

[25] Pourreza, T., Alijani, A., Maleki, V. A., Kazemi, A. "Nonlinear vibration of nanosheets subjected to electromagnetic fields and electrical current", Advances in Nano Research, 10(5), pp. 481–491, 2021.
https://doi.org/10.12989/anr.2021.10.5.481

[26] Pourreza, T., Alijani, A., Maleki, V. A., Kazemi, A. "Nonlinear vibrations of graphene nanoplates with arbitrarily orientated crack located in magnetic field using nonlocal elasticity theory", International Journal of Structural Integrity, 16(2), pp. 355–383, 2025.
https://doi.org/10.1108/IJSI-10-2024-0178

[27] Rahmani, O., Khalili, S. M. R., Malekzadeh, K., Hadavinia, H. "Free vibration analysis of sandwich structures with a flexible functionally graded syntactic core", Composite Structures, 91(2), pp. 229–235, 2009.
https://doi.org/10.1016/j.compstruct.2009.05.007

[28] Rahmani, O., Khalili, S. M. R., Malekzadeh, K. "Free vibration response of composite sandwich cylindrical shell with flexible core", Composite Structures, 92(5), pp. 1269–1281, 2010.
https://doi.org/10.1016/j.compstruct.2009.10.021

[29] Dastjerdi, S., Abbasi, M., Yazdanparast, L. "A new modified higher-order shear deformation theory for nonlinear analysis of macro- and nano-annular sector plates using the extended Kantorovich method in conjunction with SAPM", Acta Mechanica, 228(10), pp. 3381–3401, 2017.
https://doi.org/10.1007/s00707-017-1872-x

[30] Kheirikhah, M. M., Khalili, S. M. R., Malekzadeh Fard, K. "Biaxial buckling analysis of soft-core composite sandwich plates using improved high-order theory", European Journal of Mechanics - A/Solids, 31(1), pp. 54–66, 2012.
https://doi.org/10.1016/j.euromechsol.2011.07.003

[31] Viola, E., Tornabene, F., Fantuzzi, N. "General higher-order shear deformation theories for the free vibration analysis of completely doubly-curved laminated shells and panels", Composite Structures, 95, pp. 639–666, 2013.
https://doi.org/10.1016/j.compstruct.2012.08.005

[32] Malek, S., Gibson, L. "Effective elastic properties of periodic hexagonal honeycombs", Mechanics of Materials, 91, pp. 226–240, 2015.
https://doi.org/10.1016/j.mechmat.2015.07.008

[33] Tornabene, F., Viscoti, M., Dimitri, R., Aiello, M. A. "Higher order formulations for doubly-curved shell structures with a honeycomb core", Thin-Walled Structures, 164, 107789, 2021.
https://doi.org/10.1016/j.tws.2021.107789

[34] Salehipour, H., Shahmohammadi, M. A., Folkow, P. D., Civalek, O. "An analytical solution for vibration response of CNT/GPL/fibre/polymer hybrid composite micro/nanoplates", Mechanics of Advanced Materials and Structures, 31(10), pp. 2094–2114, 2024.
https://doi.org/10.1080/15376494.2022.2150916

[35] Tornabene, F., Viscoti, M., Dimitri, R. "On the Importance of the Recovery Procedure in the Semi-Analytical Solution for the Static Analysis of Curved Laminated Panels: Comparison with 3D Finite Elements", Materials, 17(3), 588, 2024.
https://doi.org/10.3390/ma17030588

[36] Chen, H.-Y., Ding, H., Li, S.-H., Chen, L.-Q. "The Scheme to Determine the Convergence Term of the Galerkin Method for Dynamic Analysis of Sandwich Plates on Nonlinear Foundations", Acta Mechanica Solida Sinica, 34(1), pp. 1–11, 2021. https://doi.org/10.1007/s10338-020-00208-6

[37] Lotfan, S., Anamagh, M. R., Bediz, B. "A general higher-order model for vibration analysis of axially moving doubly-curved panels/shells", Thin-Walled Structures, 164, 107813, 2021. https://doi.org/10.1016/j.tws.2021.107813

[38] Sayyad, A. S., Ghugal, Y. M. "Static and free vibration analysis of doubly-curved functionally graded material shells", Composite Structures, 269, 114045, 2021. https://doi.org/10.1016/j.compstruct.2021.114045

[39] Esmaeili, H. R., Kiani, Y. "Vibrations of graphene platelet reinforced composite doubly curved shells subjected to thermal shock", Mechanics Based Design of Structures and Machines, 52(2), pp. 650–679, 2024. https://doi.org/10.1080/15397734.2022.2120499

[40] Han, S., Ye, Q., Almadhor, A., Abbas, M. "Nonlinear size-dependent aerodynamics of axially reinforced doubly curved micropanel with GPLs: Application of innovative artificial neural network model", Mechanics of Advanced Materials and Structures, 31(26), pp. 8136–8160, 2024. https://doi.org/10.1080/15376494.2023.2254760

[41] Wang, T., Wang, L., Ma, Z., Hulbert, G. M. "Elastic analysis of auxetic cellular structure consisting of re-entrant hexagonal cells using a strain-based expansion homogenization method", Materials & Design, 160, pp. 284–293, 2018. https://doi.org/10.1016/j.matdes.2018.09.013

[42] Hosseini, R., Babaei, M., Naddaf, A. "The influences of various auxetic cores on natural frequencies and forced vibration behavior of sandwich beam fabricated by 3D printer based on third-order shear deformation theory", Journal of Computational Applied Mechanics, 54(2), pp. 285–308, 2023. https://doi.org/10.22059/jcamech.2023.359090.831

[43] Ebrahimi, F., Dabbagh, A. "Vibration analysis of fluid-conveying multi-scale hybrid nanocomposite shells with respect to agglomeration of nanofillers", Defence Technology, 17(1), pp. 212–225, 2021. https://doi.org/10.1016/j.dt.2020.01.007

[44] Reddy, J. N. "Mechanics of Laminated Composite Plates and Shells: Theory and Analysis", CRC Press, 2003. ISBN 9780429210693 https://doi.org/10.1201/b12409

[45] Sharafkhani, N., Orwa, J. O., Adams, S. D., Long, J. M., Lissorgues, G., Rousseau, L., Kouzani, A. Z. "An Intracortical Polyimide Microprobe With Piezoelectric-Based Stiffness Control", Journal of Applied Mechanics, 89(9), 091008, 2022. https://doi.org/10.1115/1.4054979

[46] Shabani, R., Sharafkhani, N., Gharebagh, V. M. "Static and dynamic response of carbon nanotube-based nano-tweezers", International Journal of Engineering, 24(4), pp. 377–386, 2011. https://doi.org/10.5829/idosi.ije.2011.24.04a.06

[47] Madinei, H., Rezazadeh, G., Sharafkhani, N. "Study of structural noise owing to nonlinear behavior of capacitive microphones", Microelectronics Journal, 44(12), pp. 1193–1200, 2013. https://doi.org/10.1016/j.mejo.2013.08.003

[48] Rezaee, M., Sharafkhani, N., Shervani Tabar, M. T. "Dynamic behavior of a micro-beam subjected to voltage and fluid flow as a micro vortex generator", Amirkabir Journal of Mechanical Engineering, 52(8), pp. 2231–2242, 2018.

[49] Nasrabadi, M., Sevbitov, A. V., Maleki, V. A., Akbar, N., Javanshir, I. "Passive fluid-induced vibration control of viscoelastic cylinder using nonlinear energy sink", Marine Structures, 81, 103116, 2022. https://doi.org/10.1016/j.marstruc.2021.103116

[50] Shabani, R., Sharafkhani, N., Tariverdilo, S., Rezazadeh, G. "Dynamic analysis of an electrostatically actuated circular microplate interacting with compressible fluid", Acta Mechanica, 224(9), pp. 2025–2035, 2013. https://doi.org/10.1007/s00707-013-0877-3

[51] Rezaee, M., Sharafkhani, N. "Out-of-plane vibration of an electrostatically actuated microbeam immersed in flowing fluid", Nonlinear Dynamics, 102(1), pp. 1–17, 2020. https://doi.org/10.1007/s11071-020-05882-2

[52] Rezaee, M., Fathi, R., Maleki, V. A. "Dynamic analysis and uncertainty modeling of viscoelastic beam response to fluid stimulation: Insights into nonlinear effects and velocity uncertainties", Applied Ocean Research, 157, 104487, 2025. https://doi.org/10.1016/j.apor.2025.104487

[53] Rezaee, M., Arab Maleki, V. "An analytical method for dynamic analysis of fluid conveying viscoelastic pipes", Iranian Journal of Mechanical Engineering Transactions of ISME, 21(1), pp. 6–29, 2019.

[54] Maleki, V.A., Mohammadi, N. "Buckling analysis of cracked functionally graded material column with piezoelectric patches", Smart Materials and Structures, 26(3), 035031, 2017. https://doi.org/10.1088/1361-665X/aa5324

[55] Sharan, N. "Vibration and stability of laminated composite doubly curved shells by a higher order shear deformation theory", MSc Thesis, National Institute of Technology, Rourkela, 2011. [online] Available at: https://scispace.com/pdf/vibration-and-stability-of-laminated-composite-doubly-curved-25b0ispkb3.pdf [Accessed: 20 December 2025]

[56] Librescu, L., Khdeir, A. A., Frederick, D. "A shear deformable theory of laminated composite shallow shell-type panels and their response analysis I: Free vibration and buckling", Acta Mechanica, 76(1), pp. 1–33, 1989. https://doi.org/10.1007/BF01175794